Earth and Planetary Science Letters 419 (2015) 111–124

Contents lists available at ScienceDirect

Earth and Planetary Science Letters

www.elsevier.com/locate/epsl

The evolution of climatically driven weathering inputs into the western Arctic Ocean since the late Miocene: Radiogenic isotope evidence

Veit Dausmann [a,*,1], Martin Frank [a], Christopher Siebert [a], Marcus Christl [b], James R. Hein [c]

[a] GEOMAR Helmholtz Center for Ocean Research Kiel, Wischhofstr. 1-3, D-24148 Kiel, Germany
[b] ETH Zurich, Laboratory of Ion Beam Physics, Otto Stern Weg 5, CH-8093 Zurich, Switzerland
[c] U.S. Geological Survey, 400 Natural Bridges Dr., Santa Cruz, CA 95060, United States

ARTICLE INFO

Article history:
Received 13 November 2014
Received in revised form 26 February 2015
Accepted 5 March 2015
Available online xxxx
Editor: J. Lynch-Stieglitz

Keywords:
paleoceanography
paleoclimate
Arctic Deep Water
radiogenic isotopes
glacial weathering
onset of Northern Hemisphere Glaciation

ABSTRACT

We present the first continuous records of dissolved radiogenic neodymium, hafnium, and lead isotope compositions of deep waters in the western Arctic Ocean, spanning the time from the late Miocene to the present. The data were obtained from three hydrogenetic ferromanganese (Fe–Mn) crusts recovered from seamounts along the northernmost edge of the Northwind Ridge in the Canada Basin from water depths of 2200, 2400, and 3600 m. Dating the crusts using cosmogenic ^{10}Be documents undisturbed present-day growth surfaces and yields growth rates between 27 and 2.2 mm/Myr. The Nd (Hf) isotope time series of the three crusts show similar evolutions from ε_{Nd} (ε_{Hf}) of −8.5 (+4) in the oldest parts to −11.5 (−4) at the surfaces and a pronounced trend to less radiogenic values starting at ~4 Ma. This coincided with a trend of the Pb isotope evolution towards more radiogenic ^{206}Pb/^{204}Pb, ^{207}Pb/^{204}Pb, and ^{208}Pb/^{204}Pb. It is inferred that climatically controlled changes in weathering regime and sediment transport along the North American continent were responsible for the major change of the radiogenic isotope composition of the Arctic Deep Water (ADW) in the Canada Basin. Based on these records we conclude that weathering inputs from the North American continent linked to enhanced glacial conditions started to increase and to influence the radiogenic isotope composition of ADW ~4 million years ago and were further intensified at ~1 Ma. These new time series differ markedly from the radiogenic isotope evolution of Arctic Intermediate Water recorded on the Lomonosov Ridge and suggest that much larger isotopic differences between the water masses of the Arctic Ocean than today prevailed in the past.

1. Introduction

Unraveling the oceanographic history of the Arctic Ocean and the evolution of weathering inputs from the surrounding continents, which have responded sensitively to local and global environmental changes (e.g. Moran et al., 2006), is of major importance for understanding the mechanisms driving global climatic changes. While there is evidence for extended periods of time with a perennial sea ice cover of the Arctic Ocean since 44 Ma and continuous perennial sea ice since about 36 Ma (Darby, 2014) the onset of Northern Hemisphere Glaciation (NHG) and its intensification in the late Pliocene between 2.4 and 2.9 Ma (e.g., Shackleton et al., 1984; Raymo, 1994; Zachos et al., 2001; Flesche Kleiven et al., 2002) was accompanied by the build-up of major ice sheets on the continents surrounding the Arctic Ocean (Polyak et al., 2001; Moran et al., 2006). As a consequence of enhanced glacial conditions a transition of the weathering regimes on land towards increased mechanical denudation occurred (e.g. Riebe et al., 2004).

Previous studies have invoked regional tectonic forcing (Matthiessen et al., 2009; Knies et al., 2014) and changes in ocean circulation in the North Atlantic linked to the closure of the Isthmus of Panama (Driscoll and Haug, 1998) as well as moisture export from the subarctic Pacific (Haug et al., 2005) as possible triggers for the onset of Plio-Pleistocene circum-Arctic glaciation. However, the exact temporal and spatial evolution of this pronounced climatic change is not well constrained from the marine sedimentary record in the Arctic Ocean as a consequence of the paucity of long sedimentary records. The only available record covering the past 55 million years was recovered dur-

* Corresponding author.
E-mail address: vdausmann@geomar.de (V. Dausmann).
[1] Tel.: +49 431 600 2259; fax: +49 431 600 2928.

http://dx.doi.org/10.1016/j.epsl.2015.03.007
0012-821X/

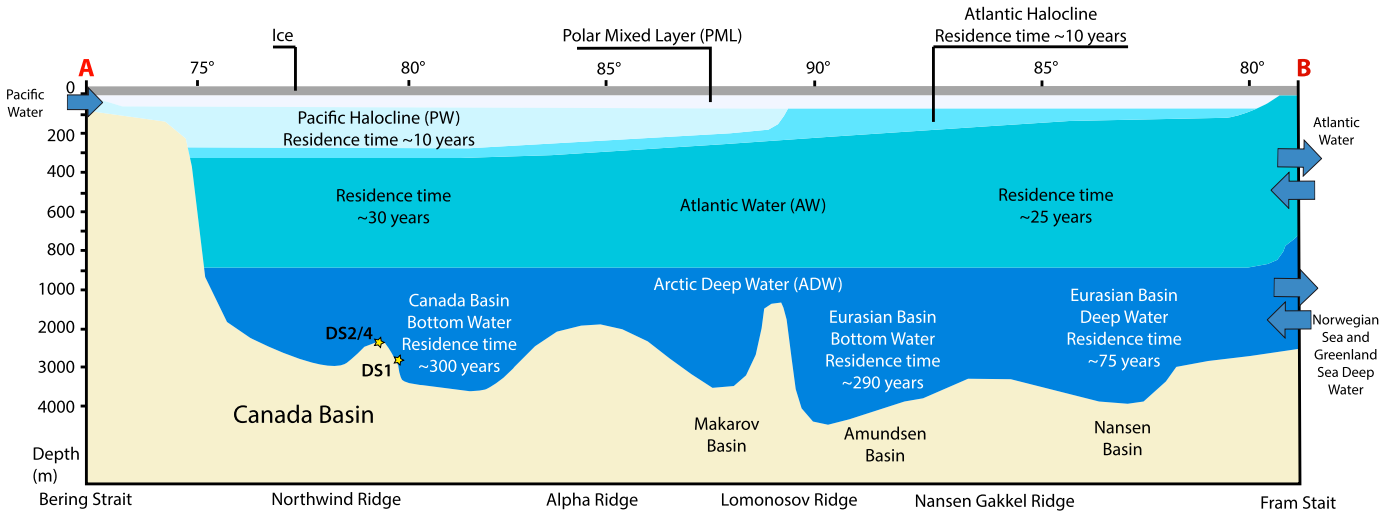

Fig. 1. Schematic transect across the Arctic Ocean including major water masses (modified from AMAP, 1998). Approximate positions of the samples on the Northwind Ridge are indicated. Residence times of water masses have been adopted from Bönisch and Schlosser (1995).

ing IODP Leg 302, the Arctic Coring Expedition (ACEX), from an intermediate water depth of 1200 m on the Lomonosov Ridge and is interrupted by a short and a long hiatus between 9.4 and 11.6 Ma and 18.2 and 44.4 Ma, respectively (Moran et al., 2006; Backman et al., 2006, 2008). Several studies have analyzed climatically driven changes in the provenance of the sediments supplied to the core location. Haley et al. (2008b) for example applied radiogenic isotopes to demonstrate that detrital inputs in the central Arctic Ocean have been linked to climatic forcing of weathering on the Eurasian continental margin, whereas März et al. (2010) defined geochemical units (based on major and trace elements) representing changes in detrital provenance, as well as in paleoenvironmental and diagenetic processes. Other than that only Pliocene Arctic sediments have been accessible from some very low sedimentation rate locations such as in the vicinity of the Alpha Ridge (e.g. Winter et al., 1997), for which the age models are, however, not well constrained due to the absence of carbonate microfossils. Recent evidence suggested that the true maximum ages of these records are much younger than initially published (e.g. Jakobsson et al., 2000) but there is still debate on the age models of sediments in the western Arctic Ocean (e.g. Sellén et al., 2009).

Here we present the first combined seawater-derived radiogenic isotope records of Nd, Hf, and Pb obtained from three hydrogenetic Fe–Mn crusts from the Northwind Ridge in the Canada Basin, which are condensed chemical sediments and reflect the continuous evolution of weathering regimes and erosional inputs for the period from the late Miocene (7 Ma) to the present.

1.1. Tracing weathering inputs and water-mass mixing with radiogenic isotopes

The main source for dissolved radiogenic Nd, Hf and Pb in the ocean is weathering of continental rocks and island arcs, the signatures of which are transferred to the ocean via dissolved and particulate phases of rivers (cf. Frank, 2002). Furthermore, hydrothermal inputs can be significant sources of Pb and Hf close to vent sites (van de Flierdt et al., 2004). Partial dissolution of and exchange with shelf sediments has recently been identified as another input source for dissolved oceanic Nd, which may even be more important than riverine inputs (Lacan and Jeandel, 2005b; Arsouze et al., 2009; Rempfer et al., 2012). Having average residence times in seawater on the order of 400–2000 years and thus shorter than or similar to the global ocean mixing time, Nd and Hf isotopes are not distributed homogeneously and can in the case of Nd be applied as quasi-conservative tracers of present and past water masses and their mixing, at least on basin-wide scales (cf. Piepgras and Wasserburg, 1987; Jeandel, 1993; Jeandel et al., 1995). Pb isotopes are suitable for the reconstruction of local inputs from land and their short distance mixing due to the shorter average residence time of Pb (50–200 years) in seawater (cf. von Blanckenburg et al., 1996).

In contrast to Nd, Hf weathers incongruently which results in more radiogenic Hf isotope compositions of rivers and seawater than expected from the corresponding Nd isotope signatures forming the so-called seawater array (Albarède et al., 1998; Chen et al., 2013; David et al., 2001; Zimmermann et al., 2009a, 2009b; Rickli et al., 2009). This observation is mainly a consequence of the "zircon effect", which is a consequence of the fact that most of the unradiogenic Hf in a rock is bound in highly weathering resistant zircons (White et al., 1986). The zircon effect is most likely not the sole reason for these signatures and differential weathering of the highly radiogenic zircon-free Hf fraction also plays a significant role in controlling seawater Hf isotope compositions (Chen et al., 2011; Bayon et al., 2009; Rickli et al., 2012).

The reconstruction of past deep-ocean circulation and weathering inputs using radiogenic isotopes on millennial time scales has been achieved by analyzing various phases of marine sediments, such as fish teeth (e.g. Martin and Haley, 2000) or Fe–Mn coatings of particles or foraminifera (e.g. Rutberg et al., 2000; Roberts et al., 2010). Hydrogenetic Fe–Mn crusts, which are chemical sediments that accrete at very low growth rates of generally 1–10 mm/Myr directly from seawater in areas of reduced or absent clastic sedimentation, enabled the investigation of the isotopic evolution on million year time scales in all major ocean basins (e.g. Ling et al., 1997; Burton et al., 1997, 1999; O'Nions et al., 1998; Reynolds et al., 1999; Frank et al., 2002). Due to the lack of long sedimentary records our new Arctic Ocean crust records offer important new insights.

1.2. Hydrography of the Arctic Ocean

The Arctic Ocean is a strongly stratified and semi-enclosed basin (Fig. 1) with approximately 35% of its extent underlain by shallow continental shelves. The uppermost 50 m of the Arctic water column, termed the Polar Mixed Layer (PML), is characterized by temperatures as low as −1.7 °C as a function of highly variable freshwater supplies originating from seasonally chang-

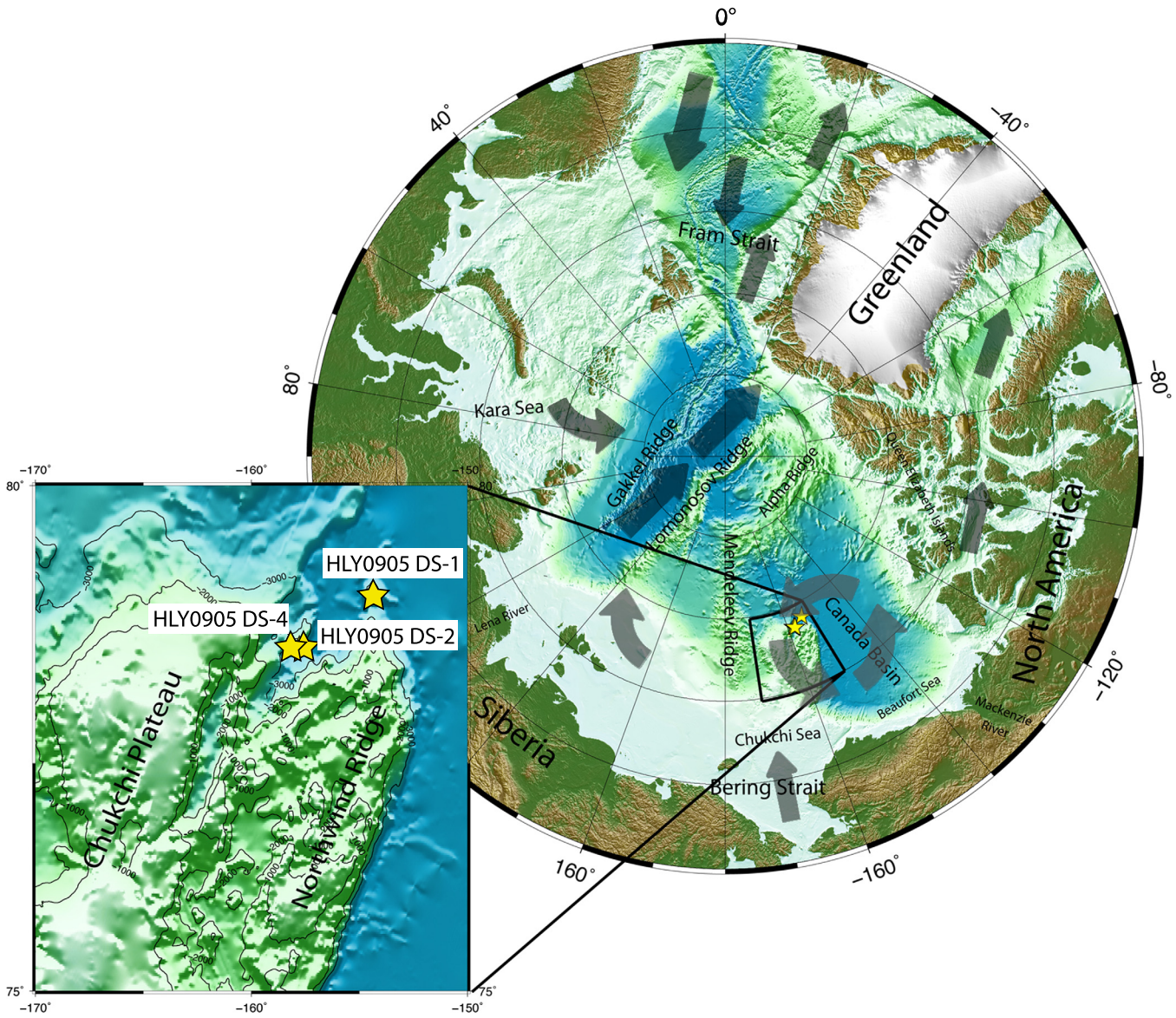

Fig. 2. Bathymetric map showing the locations of the crust samples of this study. The arrows schematically indicate modern surface circulation.

ing inputs from sea ice melting and from the discharge of large rivers (Ob, Yenisey, Khatanga, Lena, McKenzie) which together produce ~10% of the global river runoff (Stein, 2000). Below the PML the cold and very stable halocline layer between ~50 and ~200 m water depth is mainly a consequence of salt rejection during sea ice formation in open waters near the shelves (Aagaard et al., 1981). It almost completely inhibits vertical exchange of waters and thus convective heat transfer from the waters below. The relatively warm intermediate and deep waters in the Arctic Ocean are essentially of Atlantic origin (e.g., Andersson et al., 2008; Aagaard et al., 1985). As a consequence of the limited exchange with the surface waters and with the global ocean, deep and bottom waters of the Arctic basins have relatively long residence times on the order of 300 years (Bönisch and Schlosser, 1995) (see Fig. 1).

However, there are additional processes, such as brine formation near the shelves and exchange processes with the continental margins that also affect the radiogenic isotope composition of the deep Arctic Ocean (Winter et al., 1997; Haley et al., 2008a, 2008b; Porcelli et al., 2009; Haley and Polyak, 2013).

2. Methods and material

The Hf, Nd and Pb isotopic records of Arctic bottom waters were obtained from sections of three Fe–Mn crusts (DS1-001, DS2-006G and DS4-006B) recovered from the flanks of seamounts (water depth 3600–2200 m) along the northernmost margin of the Northwind Ridge in the Canada Basin (see Figs. 1 and 2) during cruise HLY0905 (7 August–16 September 2009) onboard the research vessel USCGC Healy.

For Be isotope analysis used for establishing chronologies each crust section was sampled at five different depth intervals representing between 1 and 5.5 mm of crust growth (see Table 1). For the analysis of Nd, Hf and Pb isotopes the layers typically comprise 1–2 mm corresponding to about 40 mg for each sample (Table 2).

All samples for the analysis of Nd, Hf and Pb isotopes were dissolved in 6 M HCl and purified at GEOMAR using ion chromatography following established procedures (Cohen et al., 1988; Münker et al., 2001; Galer and O'Nions, 1989). Two samples of the detrital fraction of crust DS1-001 were also prepared for Nd and Hf isotope analysis (Table 2). For this purpose about 400 mg of sample material was dissolved in 6 M HCl on a hotplate over night

Table 1
Beryllium isotope composition of crusts and calculated ages. One sample of crust DS1-001 at 9–11 mm depth yielded a significantly elevated ^{9}Be concentration after repeated measurements. Most likely this sample contains a labile, Be-enriched mineral phase that results in a very low ^{10}Be/^{9}Be and thus does not represent a seawater value. This value was consequently excluded from the calculation of growth rates and the age reconstruction. Errors are given as 1σ uncertainties.

Sample	Depth [mm]	Mean depth [mm]	^{10}Be [$\times 10^{15}$ at./g]	^{9}Be [$\times 10^{7}$ at./g]	^{10}Be/^{9}Be [$\times 10^{-8}$]	$\pm$ [$\times 10^{-8}$]	Age [Ma]	$\pm$ [Ma]
DS1-001	Surface	0.5	183.4	97	1.89	0.15	0.08	0.01
DS1-001	4.5–6	5.25	158.8	135	1.18	0.08	0.80	0.06
DS1-001	9–11	10	119.2	1583	0.08	0.01		0.00
DS1-001	30–35.5	32.75	62.9	386	0.16	0.01	4.98	0.35
DS1-001	45–49.2	47.1	35.0	358	0.10	0.01	6.00	0.50
DS2-006G	Surface	0.5	355.3	163	1.66	0.11	0.06	0.00
DS2-006G	4.5–5.5	5	289.0	331	1.23	0.08	0.61	0.04
DS2-006G	4.5–5.5	10.1	181.6	337	0.77	0.05	1.23	0.09
DS2-006G	32.5–34.5	33.5	110.4	403	0.17	0.01	4.20	0.28
DS2-006G	47–50	48.5	73.3	330	0.09	0.01	5.52	0.49
DS4-006B	Surface	0.5	164.1	99	2.19	0.14	0.23	0.01
DS4-006B	3.9–5.1	4.5	218.9	178	0.87	0.06	2.07	0.14
DS4-006B	9.5–11.5	10.5	157.0	204	0.54	0.03	3.04	0.19
DS4-006B	17.5–20	18.75	65.5	376	0.27	0.02	3.41	0.22
DS4-006B	29.5–30.5	30	27.5	306	0.22	0.02	3.90	0.28

to ensure complete dissolution of the Fe–Mn-oxyhydroxide fraction, pipetted off, and further rinsed with MQ water. The detrital residues were dried, finely ground and totally digested in a mixture of concentrated HF and HNO_3 in high-pressure bombs prior to column chemistry.

Measurements were performed on a Nu Plasma Multi-collector ICP-MS at the GEOMAR in Kiel. Mass fractionation effects in the instrument were corrected using ^{146}Nd/^{144}Nd = 0.7219 and ^{179}Hf/^{177}Hf = 0.7325 following an exponential law. For Pb isotope determination a standard-sample-bracketing method was applied (Albarède et al., 2004). The external reproducibilities were estimated by repeated measurements of the standards JMC475 with a ^{176}Hf/^{177}Hf of 0.282160 (Blichert-Toft, 2008), JNdi-1 having a ^{143}Nd/^{144}Nd of 0.512115 (Tanaka et al., 2000) and NIST NBS981 that has a ^{206}Pb/^{204}Pb of 16.9405, a ^{207}Pb/^{204}Pb of 15.4963 and a ^{208}Pb/^{204}Pb of 36.7219 (Galer and Abouchami, 1998). 2σ external reproducibilities of 0.28 (ε_{Hf}), 0.21(ε_{Nd}), 0.0058 for ^{206}Pb/^{204}Pb, 0.0073 for ^{207}Pb/^{204}Pb, and 0.0251 for ^{208}Pb/^{204}Pb (n(Hf) = 14, n(Nd) = 25, n(Pb) = 24) were obtained.

The Fe–Mn material for analysis of Be isotopes was also brought into solution using 6 M HCl and split into aliquots for the separate measurement of the two Be isotopes. In order to measure the ^{10}Be concentration by isotope dilution, a known amount of a ^{9}Be carrier was added to a weighed aliquot of the leached crust solution. The sample leaches were then further purified and prepared for Accelerator Mass Spectrometry (AMS) analysis following an established method (Henken-Mellies et al., 1990; Frank et al., 1994). The ^{10}Be concentrations were measured at the AMS Tandy facility at ETH Zurich, Switzerland. The repeatedly measured ^{10}Be/^{9}Be ratios of standards were normalized to the internal AMS standard S555N with a nominal ^{10}Be/^{9}Be ratio of $87.1 \cdot 10^{-12}$ (Christl et al., 2013). The given statistical 1σ uncertainties include counting statistics and reproducibility of repeated measurements. The second set of aliquots was measured for ^{9}Be concentration using the AGILENT 7500cs ICP-MS at the Institute of Geosciences, University of Kiel, Germany following standard procedures (Garbe-Schönberg, 1993). The 1σ uncertainties of the ^{9}Be measurements are 5%.

3. Results

3.1. Be isotope profiles and age models

The ratios between cosmogenic ^{10}Be and terrestrial ^{9}Be for the surfaces of the crusts range between $1.7 \cdot 10^{-8}$ and $2.2 \cdot 10^{-8}$ (Table 1) and are significantly lower than the range of 5 to $8 \cdot 10^{-8}$ expected for present-day Arctic Deep Water (Frank et al., 2009). Potential reasons for this difference are discussed in detail in Section 4.1 and in the supplement. All samples show a continuous decrease of ^{10}Be/^{9}Be ratios with increasing depth in the crusts from which distinct average growth rates and ages were calculated based on linear regression lines through the data points and applying the ^{10}Be half-life of 1.387 Myr (Chmeleff et al., 2010; Korschinek et al., 2010) (Fig. 3, Table 1). The growth rates vary between 14 and 2.2 mm/Myr and are typical for hydrogenetic crusts, with only the oldest section of crust DS4-006B indicating an even higher growth rate. The resulting ages at the bases of the crusts are between 6.5 and 7.2 Ma. Further details on the Be isotope chronologies are provided in the supplement.

3.2. Hf isotope time series

The ε_{Hf} signatures of past seawater recorded by the three crusts range from +4.3 to −4.2 (Fig. 4a, Table 2). The ε_{Hf} values at the surfaces of the crusts are between −4.2 and −1.2. This is in broad agreement with the only available modern deep water Hf isotope composition of the Canada Basin of $+0.3 \pm 1.8$ and with the range of present day deep waters in other Arctic basins between 0 and −2 (Zimmermann et al., 2009b). All crusts show similar Hf isotope evolutions with the highest ε_{Hf} values found in the oldest sections of the crusts between 4 and 7 Ma, which thereafter became continuously less radiogenic and lowest values were reached at the surfaces. The highest gradient of change in ε_{Hf} occurred within the last million years. The detrital ε_{Hf} signatures obtained from crust DS1-001 are −11.3 for the depth interval from 0 to 15 mm and −3.2 for the interval from 60 to 75 mm depth. Two samples of crust DS1-001, one at the surface and the other at a depth of 11 mm, corresponding to ages of 0 and 1.7 Ma, yielded extremely unradiogenic ε_{Hf} values of −14.6 and −15.5 respectively. Measurements at neighboring depth intervals yielded −3.0 for a depth of 1.5 mm and −0.9 for the interval between 8 and 9 mm depth. Given that such unradiogenic values are not realistic for dissolved seawater ε_{Hf} at those time intervals but are similar to the detrital material (see Table 2), we infer that a significant amount of Hf contained in the detrital material of these two samples was partially dissolved during chemical treatment, which due to much higher concentrations in the Fe–Mn crust material did at the same time not influence the Nd and Pb isotope signatures of these samples. Consequently these two samples were excluded from the interpretations of the Hf isotope time series and will not be further discussed.

Table 2
Radiogenic isotope data of all analyzed samples. Average 2σ deviations were 0.28 for ε_{Hf}, 0.025 for $^{208}Pb/^{204}Pb$, 0.007 for $^{207}Pb/^{204}Pb$ and 0.006 for $^{206}Pb/^{204}Pb$.

Sample	Depth min [mm]	Depth max [mm]	Weight [mg]	Age [Ma]	ε_{Nd}	2σ ±	ε_{Hf}	$^{208}Pb/^{204}Pb$	$^{207}Pb/^{204}Pb$	$^{206}Pb/^{204}Pb$
DS1-001	0	1	33.5	0.1	−11.28	0.16	−14.6	38.880	15.636	18.956
DS1-001	1	2	31.3	0.2			−3.0	38.852	15.629	18.925
DS1-001	2	3	10.1	0.4	−10.56	0.16		38.696	15.600	18.771
DS1-001	4	5	32.2	0.7	−10.48	0.13	−1.2	38.757	15.615	18.837
DS1-001	6	7	9.6	1.0	−9.86	0.16		38.764	15.615	18.819
DS1-001	8	9	40.6	1.3	−10.08	0.13	−0.9	38.749	15.611	18.820
DS1-001	10.5	11.5	39.8	1.7	−9.99	0.16	−15.5	38.823	15.601	18.803
DS1-001	15	16	15.4	2.4	−9.28	0.16		38.750	15.609	18.860
DS1-001	16	18	51.9	2.6	−9.52	0.13	1.3	38.679	15.600	18.741
DS1-001	18	19	14.4	2.8	−9.26	0.16		38.735	15.616	18.755
DS1-001	18	19	25.3	2.8	−9.51	0.13	1.8	38.683	15.602	18.734
DS1-001	20	30	32.3	3.8	−9.25	0.16	1.8	38.662	15.587	18.654
DS1-001	23	32	8.8	4.2	−8.86	0.16		38.588	15.583	18.618
DS1-001	31	38.5	9.7	4.7	−8.64	0.16		38.571	15.578	18.582
DS1-001	34.8	41	37.1	4.9	−8.83	0.16	2.5	38.582	15.583	18.580
DS1-001	37	43.5	8.6	5.1	−8.81	0.16		38.613	15.589	18.591
DS1-001	39	45.5	10.5	5.2	−8.74	0.16		38.574	15.579	18.583
DS1-001	45.5	51.5	31.8	5.7	−8.98	0.16	2.8	38.583	15.581	18.616
DS1-001	54	60.5	8	6.3	−9.15	0.40		38.585	15.581	18.618
DS1-001	66	73	10.4	7.2	−9.00	0.40		38.607	15.588	18.636
DS2-006G	0	1	30.6	0.1	−11.44	0.16	−4.2	38.866	15.631	18.943
DS2-006G	1	2	47.9	0.2	−10.52	0.13	−2.6	38.801	15.622	18.890
DS2-006G	2	3	10	0.3	−11.06	0.40		38.818	15.626	18.882
DS2-006G	4	5	50.7	0.5	−10.06	0.13	−0.2	38.728	15.610	18.810
DS2-006G	5	6.2	10.6	0.7	−10.16	0.40		38.709	15.603	18.795
DS2-006G	8	9.5	18.2	1.1	−9.69	0.16	0.9	38.752	15.600	18.734
DS2-006G	8	9.5	10.7	1.1	−7.94	0.40		38.697	15.606	18.727
DS2-006G	11.5	12.5	10.5	2	−9.67	0.40		38.627	15.589	18.677
DS2-006G	14	15.5	25.1	2.4	−9.44	0.16	1.0	38.686	15.598	18.711
DS2-006G	14	15.5	10.2	2.4	−9.41	0.40		38.642	15.593	18.680
DS2-006G	17	18	13.8	2.7	−9.29	0.11		38.655	15.595	18.688
DS2-006G	20	21	9.8	3.1	−9.25	0.11		38.644	15.594	18.681
DS2-006G	23	24	23.2	3.5	−9.19	0.16	2.2	38.644	15.594	18.678
DS2-006G	26	27	31.4	3.9	−8.98	0.13	1.5	38.612	15.587	18.650
DS2-006G	29.5	32	10	4.4	−8.93	0.11		38.564	15.577	18.589
DS2-006G	39.5	41	10.7	4.6	−8.90	0.11		38.526	15.568	18.535
DS2-006G	43	44	36.7	4.9	−8.82	0.13	4.3	38.532	15.568	18.532
DS2-006G	49.3	50.7	9.6	5.4	−8.90	0.11		38.210	15.583	18.549
DS2-006G	57	59	44.5	6.2	−8.66	0.13	2.6	38.536	15.572	18.550
DS2-006G	60	63.5	34.2	6.5	−8.72	0.16	2.6	38.548	15.576	18.557
DS4-006B	0	1.5	36.9	0.3	−10.49	0.16	−1.2	38.786	15.620	18.864
DS4-006B	2	3	13	1.1	−9.93	0.40		38.695	15.604	18.776
DS4-006B	2	3	22	1.1	−9.82	0.13	0.1	38.697	15.605	18.779
DS4-006B	3	5	10.5	1.8	−9.73	0.40		38.688	15.604	18.749
DS4-006B	7	8	31.5	2.4	−9.17	0.16	1.5	38.577	15.577	18.634
DS4-006B	9	10.5	19.2	2.8	−9.07	0.40		38.612	15.589	18.653
DS4-006B	11	12	58.5	3.1	−8.94	0.13	1.5	38.611	15.588	18.655
DS4-006B	13	14.5	12.1	3.4	−8.71	0.40		38.601	15.587	18.634
DS4-006B	16	18	38	3.9	−8.75	0.16	1.7	38.613	15.591	18.636
DS4-006B	23	26.5	9.8	4.2	−8.91	0.40		38.519	15.568	18.524
DS4-006B	26.5	30	10	4.4	−8.50	0.40		38.526	15.571	18.535
DS4-006B	30	33	44.5	4.5	−8.65	0.16	2.4	38.524	15.572	18.537
DS4-006B	35	38	9.7	4.7	−8.41	0.40		38.519	15.569	18.534
DS4-006B	45	48	10.3	5.1		0.40		38.501	15.558	18.531
DS4-006B	49	50	53	5.2	−8.94	0.13	2.7	38.540	15.572	18.557
DS4-006B	57.8	61	9.7	6.2	−8.85	0.11		38.579	15.581	18.574
DS4-006B	67	70.5	10	6.5	−9.03	0.11		38.586	15.582	18.560
DS4-006B	72	73	43.3	6.7	−8.93	0.13	3.3	38.560	15.572	18.559
DS4-006B	75	77.5	38.3	6.8	−8.73	0.16	2.3	38.578	15.578	18.575
Detrital										
DS1-001	0	15	429	–	−13.50		−11.3			
DS1-001	60	75	374	–	−9.10		−3.2			

3.3. Nd isotope time series

The ε_{Nd} time series range between −8.4 and −11.4 and agree very well among the three crusts (Table 2, Fig. 4b). Similar to the Hf isotope compositions, ε_{Nd} values were constant at around −9 until about 4 Ma and then started to decrease continuously to values near −11.5 at the surface of the crust. This corresponds to an average decrease of ∼0.66 ε_{Nd} units per Myr for the period between ∼4 and ∼1 Ma and a stronger gradient thereafter. The surface ε_{Nd} values between −10.5 and −11.4 are in good agreement with the modern value for the deep Canada Basin of −11 (Porcelli et al., 2009). The detrital samples yielded an ε_{Nd} of −13.5 for the depth interval from 0 to 15 mm and −9.1 ε_{Nd} for the interval from 60 to 75 mm in crust DS1-001.

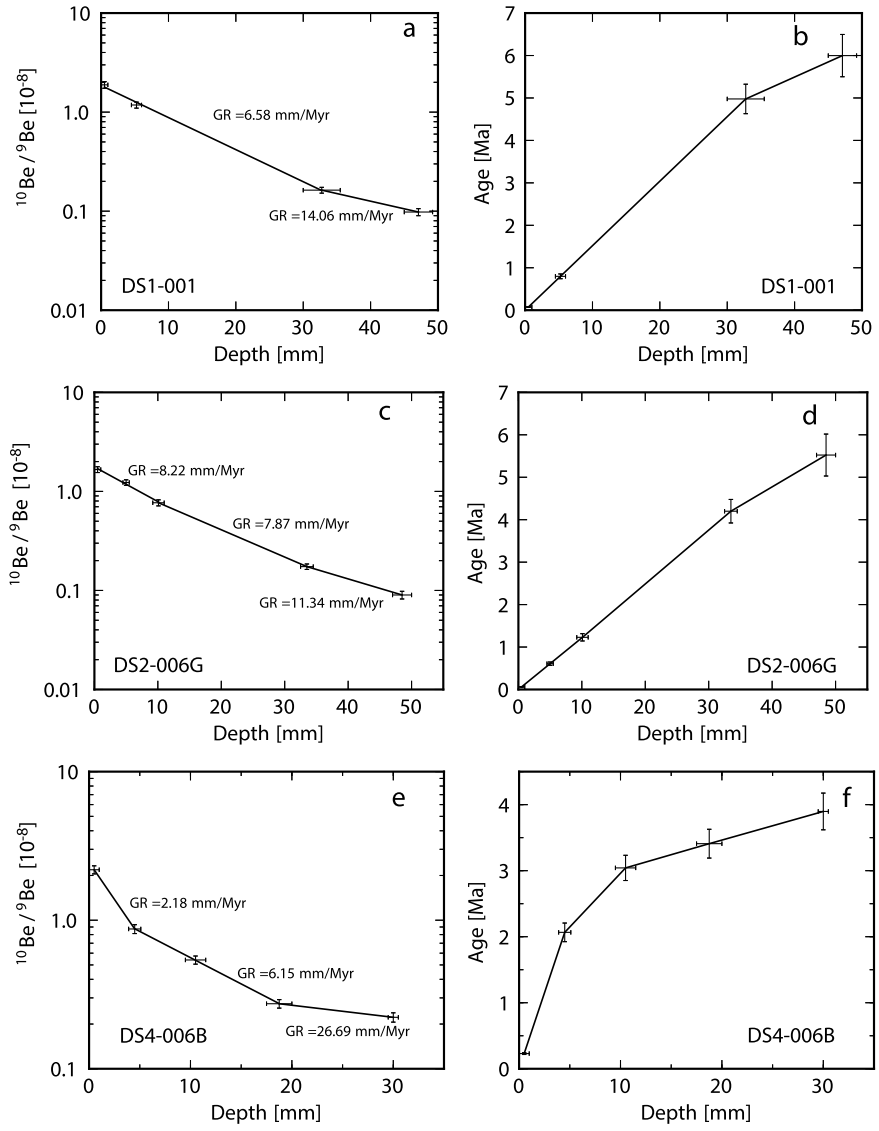

Fig. 3. Profiles of beryllium isotope ratios and calculated ages against depth [mm] for the three crusts of this study. Error bars denote the combined 2σ statistical uncertainties of the AMS and ICP-MS measurements.

3.4. Pb isotope time series

The ^{208}Pb/^{204}Pb ratios in the crusts range from 38.21 to 38.88, ^{207}Pb/^{204}Pb from 15.56 to 15.64 and ^{206}Pb/^{204}Pb from 18.52 to 18.96 (Fig. 5). There is a clear general trend for all lead isotope compositions to more radiogenic values in the younger parts of all crusts. The two crusts from shallower water depths (DS2 and DS4) show overall slightly less radiogenic Pb isotope compositions for the entire record. From approximately 7 until between 4.5 and 4 Ma, the Pb isotope signatures were essentially invariant (Fig. 5). Thereafter, the Pb isotope ratios increased step-wise. Analogous to the other isotope systems the Pb isotope time series show a higher gradient of change during roughly the last one Myr of the records.

4. Discussion

4.1. Age models based on ^{10}Be/^{9}Be

It was shown that present-day ^{10}Be/^{9}Be ratios of ADW range between 5 and $8 \cdot 10^{-8}$ (Frank et al., 2009). As mentioned above, the Be isotope ratios at the surface of all crusts from the Canada Basin are significantly lower. A growth hiatus of about 2 Myr could be a possible explanation but given that the surfaces appear unaltered and all three crust surfaces show essentially the same ^{10}Be/^{9}Be while the growth rates were different, this is considered highly unlikely. In further support of complete records, the surface Nd isotope compositions match present deep water signatures very well. Since the sampled uppermost millimeter of the three crusts integrates between 120 and 450 kyr of crust growth based on the results described in Section 3, the measurements integrate the isotopic variation of ADW of up to the last four glacial/interglacial cycles. After age correction this still suggests that the Be isotope ratio of deep water in the Canada Basin was significantly lower than it is today during extended periods of the past several 100 kyr, implying that either the supply of ^{10}Be was significantly lower or that of ^{9}Be was higher than today. Based on sediment cores from the Alpha and Mendeleev Ridge that were independently dated using nanofossil stratigraphy (Backman et al., 2009), Sellén et al. (2009) argued that superimposed on the radioactive decay there were significant reductions in ^{10}Be supply to the sediments due to prolonged periods of denser sea ice cover resulting in very low ^{10}Be/^{9}Be ratios in Arctic sediments for the past 1 Myr, except during the Holocene. This is supported by Be isotope time

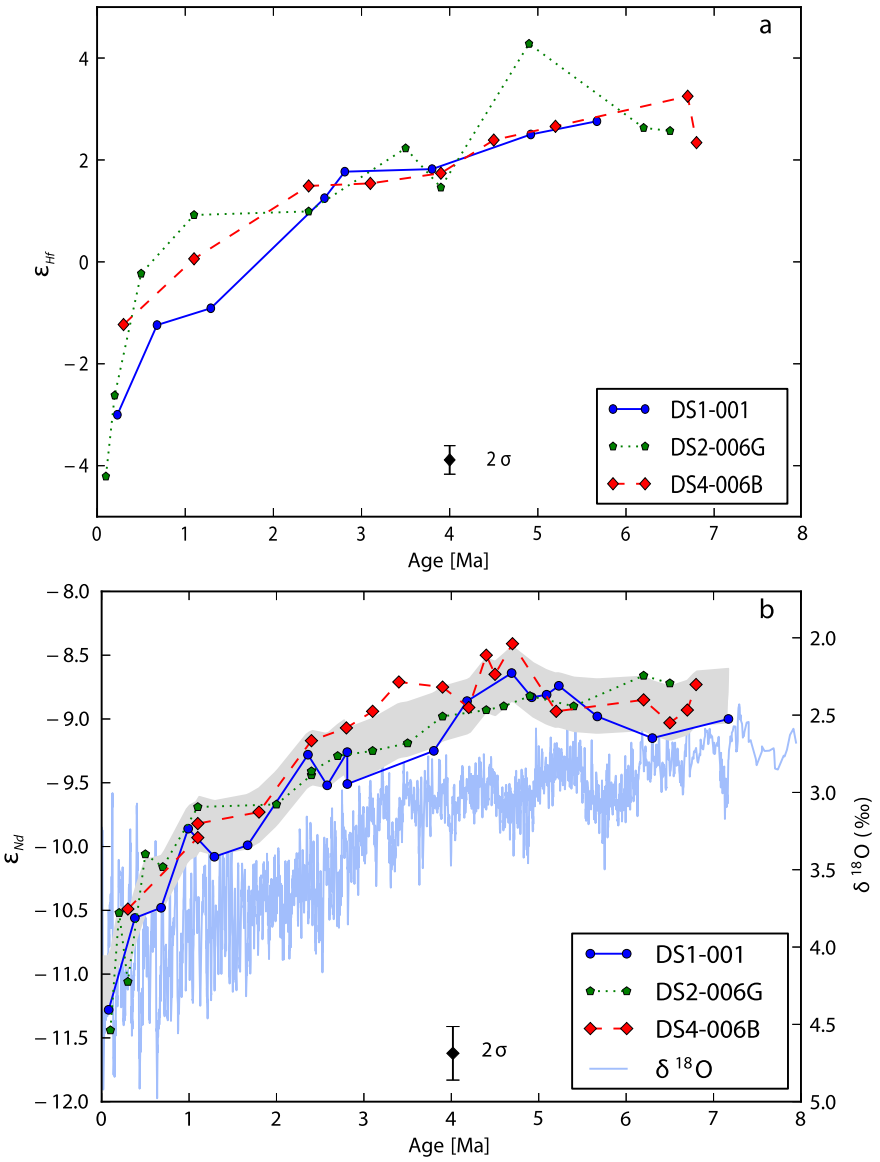

Fig. 4. (a) Hafnium and (b) neodymium isotope time series of all three crusts. The error bar denotes the 2σ external reproducibility of the MC-ICMS measurements. In (b) the area shaded in gray represents the mean of the three crusts including 1 standard deviation, while the light blue line represents the globally stacked benthic foraminiferal $\delta^{18}O$ record (Zachos et al., 2001). ε values correspond to the normalized differences of the sample ratio from the one of the chondritic uniform reservoir (CHUR) times 10 000 with $^{143}Nd/^{144}Nd_{CHUR}$ being 0.512638 (Jacobsen and Wasserburg, 1980) and $^{176}Hf/^{177}Hf_{CHUR}$ being 0.282769 (Nowell et al., 1998). (For interpretation of the references to color in this figure legend, the reader is referred to the web version of this article.)

series from intermediate water depth on the Lomonosov Ridge in the Eurasian Basin, which also have been inferred to be shifted to low values due to the shielding effect of a nearly permanent sea ice cover (Frank et al., 2008). The thickness of sea ice varies regionally but has been shown to be highest beneath the Beaufort Gyre where it has also been shown to be oldest and where the crusts analyzed here were recovered. In support of this, Eisenhauer et al. (1994) showed that during glacial times the fluxes of ^{10}Be to Arctic sediments were lower than the modern interglacial average due to denser sea ice cover and enhanced export of ^{10}Be deposited on the sea ice via the Transpolar Drift through the Fram Strait.

Further potential influences on the Be isotope data and the Be derived age model are discussed in the supplement. For the interpretation of our radiogenic isotope data we adopt the calculations and age models in Section 3 and assume that initial $^{10}Be/^{9}Be$ ratios of $\sim 2 \cdot 10^{-8}$ are realistic for our dating approach and represent the realistic integrated average initial glacial-interglacial deep water Be isotope composition of the Arctic Ocean, which still requires a substantially lower glacial $^{10}Be/^{9}Be$ signature than today. Remaining uncertainties of the age models linked to the Be isotope evolution of the deep Arctic Ocean can only be constrained by future $^{10}Be/^{9}Be$ records with independent age models.

4.2. Weathering controlled changes in the radiogenic isotope evolution of ADW

Fig. 7 illustrates the pronounced shift towards less radiogenic Nd and Hf isotope signatures and more radiogenic Pb isotope signals observed in our Arctic Fe–Mn crust time series, which closely resembles records obtained from crusts in the North Atlantic (e.g., Burton et al., 1997, 1999; O'Nions et al., 1998; Reynolds et al., 1999; Piotrowski et al., 2000). The latter records documented a continuous shift in the Nd and Hf isotopic composition of North Atlantic Deep Water (NADW) (from −11 to about −13 for ε_{Nd}, from 3 to −1 for ε_{Hf}) which occurred after 4 Ma, while changes in $^{206}Pb/^{204}Pb$ (from ∼18.9 to ∼19.3) only started after 3 Ma in

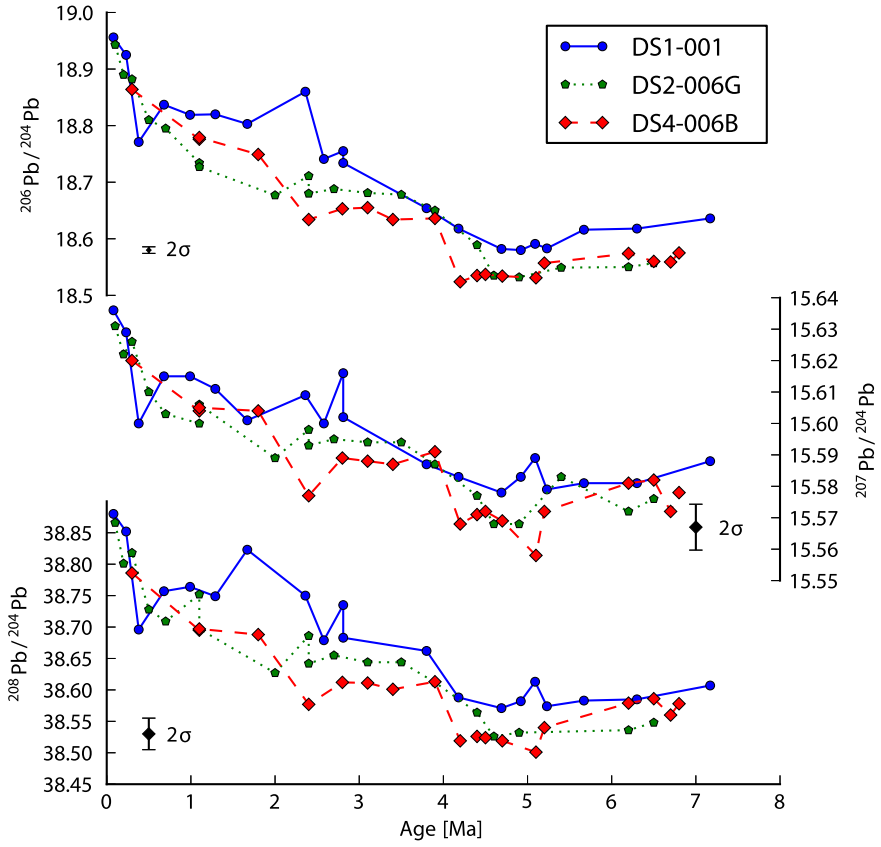

Fig. 5. Lead isotope time series of all three crusts. The error bar denotes the 2σ external reproducibility of the MC-ICMS measurements.

the NW Atlantic (Reynolds et al., 1999) and after 4 Ma in the NE Atlantic (Abouchami et al., 1999; Muiños et al., 2008). Despite a systematic isotopic offset between the records from the two basins caused by the prevailing respective water mass compositions the similarity of the patterns of the time series and of the amplitudes of the isotopic compositions recorded by the Arctic crusts to those from the Atlantic suggest that the processes that controlled the changes of the radiogenic isotope compositions of NADW and ADW were similar. Furthermore, the co-evolution of the two basins supports the integrity of our age model.

Burton et al. (1997) argued that an increasing contribution of deep waters formed in the Labrador Sea, which today has elevated Nd concentrations and ε_{Nd} values as low as −26 in the Baffin Bay (Stordal and Wasserburg, 1986), in combination with the closure of the Isthmus of Panama, which inhibited the admixture of radiogenic Pacific waters, explains the Nd and Pb isotope records of the North Atlantic Fe–Mn crusts. This mechanism cannot account for isotopic changes of the same amplitude in the Arctic Ocean. Later, von Blanckenburg and Nägler (2001) argued that the intensification of Northern Hemisphere Glaciation (INHG) resulted in a change in weathering regime and weathering inputs in the subpolar and polar regions, which is a more likely explanation for the observed isotopic variations. The combination of overall enhanced mechanical erosion increasing the influx of eroded material and glacial/interglacial alternations between predominantly chemical and physical continental weathering conditions (Vance et al., 2009) supplied unradiogenic Nd and Hf and, particularly, radiogenic Pb isotope signatures from the surrounding continental shields of Canada and Greenland to the North Atlantic and Arctic Oceans. The role of incongruent weathering for Hf and Pb isotopes is especially important as a consequence of enhanced mechanical weathering. Leaching experiments showed that radiogenic Pb is preferentially released from fresh mineral surfaces of mechanically weathered rocks (Erel et al., 1994; von Blanckenburg and Nägler, 2001; Crocket et al., 2012). Thus the freshly weathered material provides a labile pool of radiogenic Pb isotopes hosted predominantly by accessory phases, which have experienced radiation damage and/or are rich in U and Th (Erel et al., 1994; Silver et al., 1984).

In contrast to Pb, incongruent weathering of Hf isotopes is mainly the result of the zircon effect. However, during enhanced physical erosion in Northern Canada and Greenland since the INHG, increased amounts of zircons have been mechanically destroyed and finely ground and may thus have released a fraction of their unradiogenic Hf to dissolution. More congruent weathering with greater influence of physical weathering is expected to produce combined Nd/Hf isotope compositions closer to the terrestrial array (cf. van de Flierdt et al., 2002; Gutjahr et al., 2014). In support of this, direct measurements of present day (Zimmermann et al., 2009b) and past Arctic seawater data obtained from leachates of authigenic Fe–Mn coatings on sediment particles in a core from the Lomonosov Ridge (Chen et al., 2012) plot well below the seawater array in ε_{Hf}–ε_{Nd} space (Fig. 6).

4.3. Sources of radiogenic isotopes in ADW

4.3.1. North Atlantic versus pacific contributions to ADW

ADW is primarily supplied from the northern North Atlantic and the Nordic Seas via the Fram Strait (Andersson et al., 2008). It can to some extent be isotopically altered due to shelf–water interactions along the shelf margins of each of the sub-basins of the Arctic Ocean (Andersson et al., 2008; Porcelli et al., 2009). The processes involved in shelf–water interactions are not well constrained but there is clear evidence for isotopic exchange effects on Nd and probably also on Hf isotopes on the shelves of Siberia and Canada (Porcelli et al., 2009; Zimmermann et al., 2009b). However, present day ADW in the central Canada Basin ($\varepsilon_{Nd} \sim -11$) closely

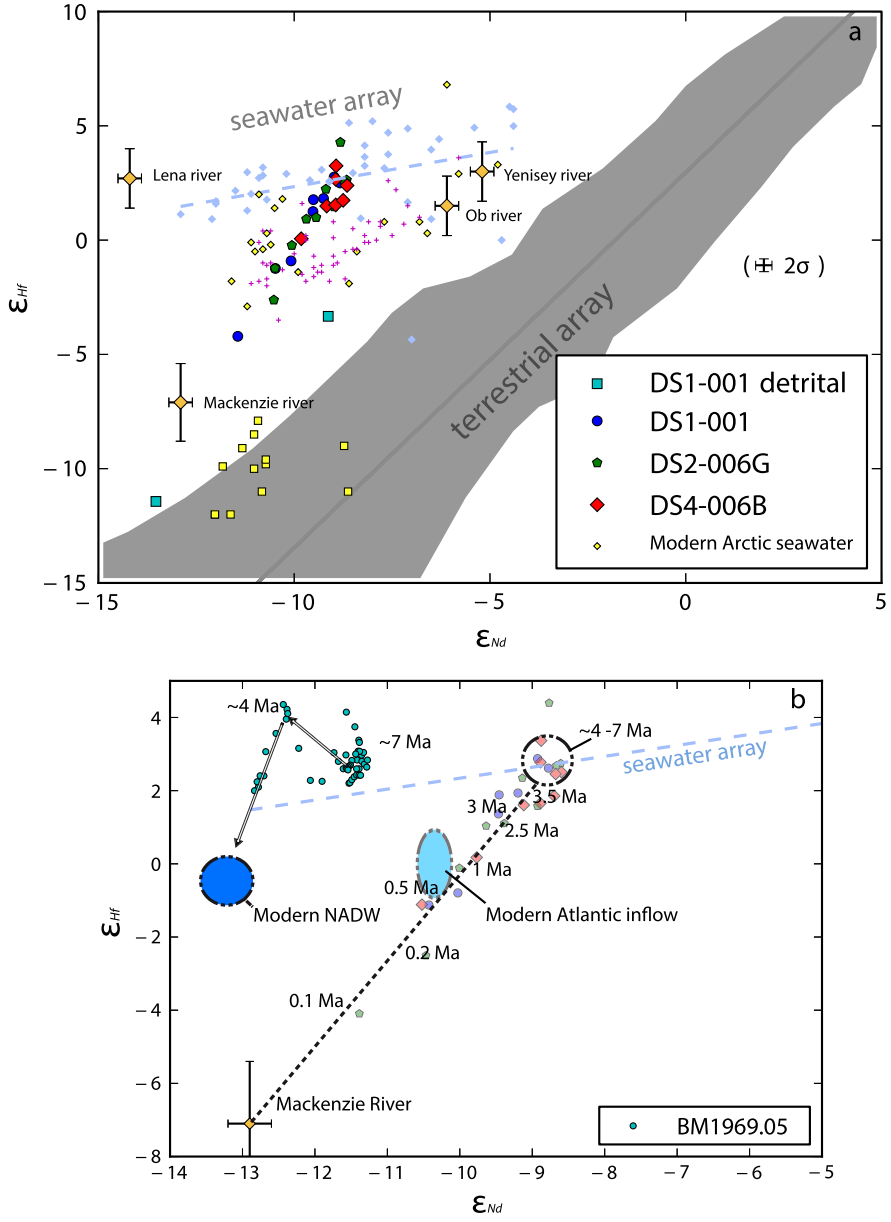

Fig. 6. ε_{Hf} versus ε_{Nd} of Arctic waters and sediments. The error bars denote the 2σ external reproducibility of the ε_{Hf} and ε_{Nd} measurements. (a) The shaded area represents the global terrestrial array (Vervoort et al., 1999). Light blue diamonds and dashed line represent the global seawater array defined by the Fe–Mn crust and seawater data (Albarède et al., 1998). The purple crosses represent the leached authigenic fraction sediment data from the Lomonosov Ridge, while the yellow squares represent the corresponding detrital fraction (Chen et al., 2012). The yellow diamonds represent data for modern seawater from the major basins of the Arctic Ocean and the large yellow diamonds denote compositions of major rivers (Zimmermann et al., 2009a). (b) ε_{Hf} versus ε_{Nd} of the three Fe–Mn crusts and the isotopic evolution of NADW based on North Atlantic crust BM1969.05. The modern Arctic inflow was characterized by Porcelli et al. (2009) and Zimmermann et al. (2009a). The black dashed line represents the isotopic evolution of the crusts from the Northwind Ridge over time. The Mackenzie River data are from Zimmermann et al. (2009a). Ages along the dashed line mark the temporal evolution of deep water in the Canada Basin. (For interpretation of the references to color in this figure legend, the reader is referred to the web version of this article.)

matches the North Atlantic Inflow (NAI) ($\varepsilon_{Nd} \sim -10.8$) and has probably been subject to only minor local alterations such as by brine formation and subduction of small amounts of waters with more radiogenic signatures of Pacific origin (Andersson et al., 2008; Porcelli et al., 2009). This is also supported by the Fe–Mn micronodule data of Winter et al. (1997) for the northernmost end of the Alpha Ridge in the Canada Basin.

The ε_{Nd} values for the surface layer of the sampled crusts average -11.2 ± 0.2 and are thus within the range of the values measured for recent ADW (Porcelli et al., 2009). This supports that the NAI is the main source of ADW in the Canada Basin.

On the other hand, the Pacific inflow of highly radiogenic waters seems to influence the shelf region of the Canada Basin and the shallow Chuckchi borderland (Zimmermann et al., 2009b; Porcelli et al., 2009). Any short-term inflow events of water masses with Pacific Ocean compositions to the deep Canada basin from the Chuckchi shelf area due to brine formation (Haley and Polyak, 2013) are not visible in our records due to the low temporal resolution. This suggests that the Pacific inflow via the Bering Strait has not contributed significant amounts of Nd to ADW during the last 7 Myr.

4.3.2. *Weathering inputs from the surrounding continents*

The data of Haley et al. (2008b) from the Lomonosov Ridge in the central Arctic Basin supported the idea that Pb isotope signatures in Arctic Intermediate Water (AIW) were derived from exchange with local weathering inputs mainly from Siberia. Winter et al. (1997) concluded from data from the Alpha Ridge that at

~3 Ma changes in provenance of the sediments carried by the waters and thus also the isotopic composition of the water itself coincided with a change in sediment transport mechanisms from sea ice to glacial ice caused by the development of the ice sheets on the continents. However, there is evidence that enhanced incongruent weathering during deglacial episodes (Vance et al., 2009; Gutjahr et al., 2009; Kurzweil et al., 2010) has most likely been the dominant process responsible for a shift to more radiogenic dissolved Pb isotope compositions in the western North Atlantic. von Blanckenburg and Nägler (2001) attributed the shift towards more radiogenic Pb isotope compositions beginning at ~3 Ma recorded by the Fe–Mn crusts of the northwestern Atlantic to the transition from predominantly chemical to mechanical erosion due to the expansion of the ice sheets and enhanced glacial weathering on the North American continent and Greenland. This change would have resulted in more incongruent weathering and contribution of a labile fraction of highly radiogenic Pb from the North American continent, in particular during deglaciations, to the dissolved Pb isotope budget of seawater in the Labrador Sea. We suggest that very similar processes were also responsible for the evolution of radiogenic Pb isotopes in the Canada Basin of the Arctic Ocean.

Winter et al. (1997) suggested a three end-member mixing history of the sources of sediments on the Alpha Ridge as reconstructed from detrital sediment isotope compositions over the last 5 Myr. They suggested northern Canada and the Queen Elizabeth Island regions to have been the dominant sources of ice-rafted sediments since the INHG while the Putorana Basalts were the dominant source of detrital isotope signatures on the Alpha Ridge prior to that. Seawater dissolved Pb and Nd isotopic compositions reconstructed from the oxide fractions of Fe–Mn micro-nodules in the sediments from the Alpha Ridge coincided with the isotopic variations of the detrital silicate fraction, which led Winter et al. (1997) to conclude that particulate material has been a major source of rare earth elements and Pb in the Arctic Ocean.

In the deep Canada Basin the mixture of dissolved radiogenic isotope compositions of seawater has most likely been defined by only two end members (Figs. 6 and 7). The evolution of our data in $^{207}Pb/^{204}Pb$–$^{206}Pb/^{204}Pb$ space shows a clear deviation from the Fe–Mn micro-nodule data of Winter et al. (1997) and a development away from the Siberia-dominated sediments of the Lomonosov Ridge (Haley et al., 2008b) (see supplementary material). While the data of Winter et al. (1997) show a trend towards a composition similar to North Atlantic crusts, our data suggest that a change in weathering style, favoring incongruent weathering was the dominant mechanism controlling the release of radiogenic lead in the younger part of the records. As a consequence it is impossible to determine the source region of radiogenic Pb from our data since the signatures of the source rocks are overprinted by the signal of incongruent weathering (cf. Crocket et al., 2012).

As the Nd and Hf analysis of the detrital fraction of the two samples of crust DS1-001 confirms that the material must have been derived from an old continental source, the Canadian Shield, the Appalachian and the Caledonian areas are plausible source regions for weathering inputs into the Arctic Ocean. Our radiogenic isotope data resemble a two end-member mixing relationship (cf. Fig. 6b), in this case, however, representing the continuous change in weathering regime (from predominantly chemical weathering to more physical erosion) on the North American continent after ~4 Ma.

4.3.3. Glacial weathering of Hf

As described in Section 4.2, previous studies found evidence for more congruent weathering due to enhanced mechanical release of relatively unradiogenic Hf to Arctic Intermediate Water under glacial weathering conditions since the INHG (Chen et al., 2012). Piotrowski et al. (2000) and van de Flierdt et al. (2002) described the same phenomenon for Fe–Mn crusts in the North Atlantic. For the deep-water isotope composition in the Canada Basin, these processes have had an even larger impact based on our data.

The Hf–Nd isotopic composition of ADW in the Canada Basin over the past 7 Myr as extracted from the Fe–Mn crusts evolved along a hypothetical mixing line between predominantly chemically weathered sources plotting close to the global seawater array of Albarède et al. (1998) prior to ~4 Ma and the composition of the Mackenzie River thereafter (Zimmermann et al., 2009b), the isotopic composition of which is close to the terrestrial array (see Fig. 6). Fig. 6b illustrates that Hf isotopes in ADW were most likely derived from predominantly chemically weathered sources prior to ~4 Ma. After that, dissolved Hf–Nd isotope compositions developed towards the present-day dissolved signature of the Mackenzie River water. This implies that the establishment of colder climates and development of continental ice sheets increasing physical weathering started around 4 Ma, which coincided with the onset of the release of highly unradiogenic Hf and Nd to the Arctic Ocean. Although the data of the crusts analyzed here reflect a development towards more congruent weathering conditions since the INHG they still are consistent with modern Arctic seawater, which also plots significantly below the seawater array (Zimmermann et al., 2009a). Furthermore, Zimmermann et al. (2009a) identified the Mackenzie River as a significant source of unradiogenic Hf to the Arctic Ocean. The river drains vast areas of the northern North American continent and constituted the remaining main outflow of the large Laurentide ice sheet to the Arctic Ocean in the past (Lemmen et al., 1994). Although estuarine burial seems to remove more than 50% of riverine dissolved Hf and Nd (Zimmermann et al., 2009a), the Mackenzie has most likely been an important source of unradiogenic Hf and Nd, as well as of radiogenic Pb in the ADW mixture. These isotope signals were either transferred to the deep Canada Basin through particulate input and subsequent dissolution in the deep basin, brine formation (e.g. Haley et al., 2008a), or redissolution of preformed riverine coatings from sediments of the Mackenzie River on the Canadian Shelf similar to observations near West African major river mouths (Kraft et al., 2013).

4.4. Radiogenic isotope evolution of ADW

Starting around 4 Ma the seawater isotope compositions in the deep Canada Basin developed towards the end-member best characterized by glacial weathering of rocks of northwestern North America and the Canadian Craton (Figs. 6b and 7). The steepest gradients of change occurred during the past 1 Myr indicating a further intensification of the processes controlling the release of unradiogenic Nd and Hf and radiogenic Pb, which most likely mainly occurred predominantly during deglacial periods (Foster and Vance, 2006; Vance et al., 2009) that are not resolvable in our records.

The Pb isotope evolution recorded by the crusts generally shows more short-term variability than those of Nd and Hf isotopes. Due to its shorter residence time Pb is more sensitive to changes in local weathering inputs. After ~4.5 Ma, the records suggest that contributions from a new, radiogenic source of Pb increased stepwise at ~4.2 Ma, ~2.7 and from 0.5 Ma to present (Fig. 5). This stepwise evolution was not observed in North Atlantic Pb isotope records. Together with the evidence for an earlier onset of the shift towards more radiogenic Pb isotopes (at 4.2 Ma, Figs. 5 and 7) we conclude that the Pb signatures in Arctic seawater responded more sensitively to changes in weathering inputs from the continents than the NW Atlantic. The location of the Canada basin within the semi-enclosed Arctic Ocean and its proximity to the evolving large ice sheets on northern North America and their weathering in-

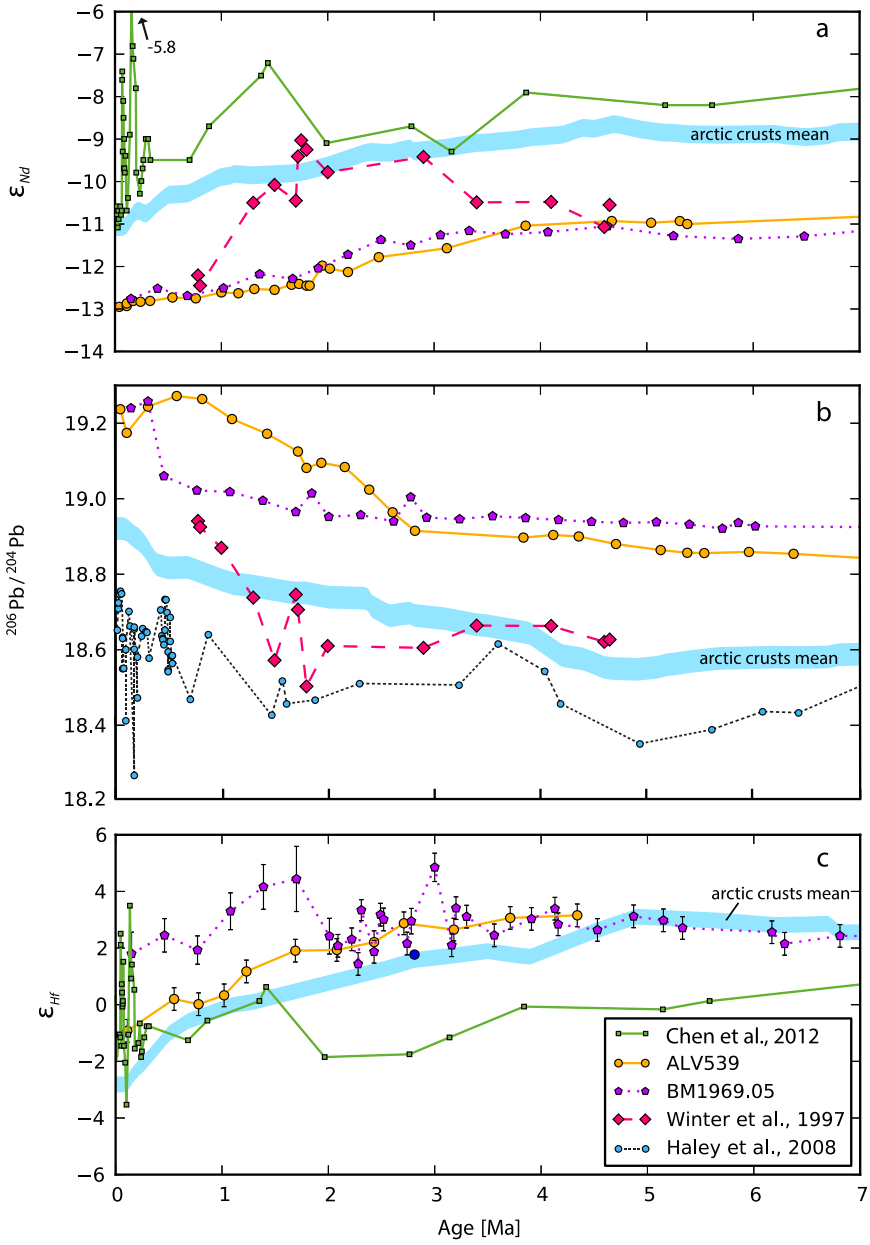

Fig. 7. Comparison of radiogenic isotope time series of Fe–Mn crusts and other records from the North Atlantic and from the Arctic Ocean. The blue areas represent the average values of the three Fe–Mn crusts of this study. ε_{Nd} values in a) for North Atlantic crusts ALV 539 and BM1969.05 are from O'Nions et al. (1998) and Burton et al. (1999). Pb isotope data of the North Atlantic crusts in b) were compiled by Reynolds et al. (1999). North Atlantic Hf isotope data in c) are from Piotrowski et al. (2000), van de Flierdt et al. (2002), and Lee et al. (1999). (For interpretation of the references to color in this figure legend, the reader is referred to the web version of this article.)

puts most likely resulted in the first signatures of enhanced glacial weathering about one million years earlier than observed in the NW Atlantic Ocean, possibly caused by initial cooling and small waxing and waning ice sheets. The radiogenic isotope signatures were most probably supplied to the Arctic Ocean to a significant extent by the Mackenzie River. The Nd and Hf isotope compositions of the detrital fractions extracted from crust DS1-001 support a Mackenzie River origin of the particulate weathering contributions for the past about 2 Myr represented by the younger detrital sample, whereas the older sample indicates contributions from other more radiogenic source areas, such as Siberia or the northern Rocky Mountains.

NADW and/or its precursors experienced an isotopic evolution similar to ADW in the Canada Basin during the past 7 Myr. An average Arctic Ocean ε_{Hf} value of +0.5, albeit with a very large uncertainty (Zimmermann et al., 2009b) together with an ε_{Nd} of −11 (Porcelli et al., 2009) reflect the modern Canada Basin deep-water signatures (Fig. 6b). At 7 Ma NADW had an ε_{Nd} signature of ∼−11.5 and an ε_{Hf} of ∼+3 while its modern ε_{Nd} is ∼−13.5 and ε_{Hf} is ∼−1 (Figs. 7a and 1c). Our data show that ADW in the deep Canada Basin had an average ε_{Nd} signature of ∼−9 and an average ε_{Hf} of +3 between 7 and 4 Ma, whereas the crust surfaces yield an ε_{Nd} signature of ∼−11 and an ε_{Hf} signature of ∼−3. The amplitudes of the ε_{Nd} changes in NADW and ADW between 7 Ma and today were similar (∼2 to 3ε_{Nd} units, Fig. 7a), whereas the change of ε_{Hf} values in the Canada Basin of up to 8ε_{Hf} units (Fig. 7c) was apparently somewhat larger than in the North Atlantic, which is probably due to the proximity of the Arctic crusts to the weathering sources and the restricted deep water exchange of the Arctic basin.

The overall similarity in radiogenic isotope evolution of the North Atlantic and the Arctic Ocean leads to the interpretation that

both regions experienced similar changes in weathering inputs as a consequence of the change in weathering regime on the adjacent continents, consistent with previous considerations based on comparison of the Canada Basin micro-nodule data of Winter et al. (1997) and the North Atlantic Fe–Mn crust time series (O'Nions et al., 1998). The direct transfer of these isotopic changes from the North Atlantic to the Canada Basin of the Arctic Ocean via water-mass mixing was most likely of subordinate importance due to the long distance along which weathering inputs from land and admixture of other water masses must have occurred. NW Atlantic deep waters were most likely influenced by additional weathering inputs and mixing with other water masses on their way from its source regions into the Arctic Ocean (Lacan and Jeandel, 2004, 2005a; Andersson et al., 2008). Thus weathering and continental input processes, most probably linked to the establishment of the Laurentide Ice Sheet, that have affected the western North Atlantic Ocean have also controlled the Canada Basin of the Arctic Ocean, although they resulted in different absolute radiogenic isotope ratios as a consequence of the overall different radiogenic isotope compositions of the waters in the two basins.

Comparison of our data and those of Winter et al. (1997) from the deep Canada Basin with the radiogenic isotope evolution of shallow AIW (1200 m water depth) on the Lomonosov Ridge (Haley et al., 2008a, 2008b; Chen et al., 2012) shows pronounced differences in the isotopic evolution of the bottom water masses. The Nd and Hf isotope variability of AIW was closely linked to the inflow of Atlantic waters (NAI) and changes in the intensity of brine formation on the Siberian shelf (Haley et al., 2008a; Chen et al., 2012). The detrital inputs were at the same time clearly dominated by Eurasian and Siberian sources as reflected by the detrital radiogenic isotope compositions of Nd, Sr, and Pb, as well as seawater isotope compositions of particle reactive Pb of AIW (Haley et al., 2008b). This heterogeneity of Arctic water masses throughout the last 7 Myr is in pronounced contrast to the small present-day dissolved radiogenic isotope variability Andersson et al., 2008; Zimmermann et al., 2009b; Porcelli et al., 2009 and supports markedly different processes that controlled their distributions in the different sub-basins of the Arctic Ocean under changing climatic conditions, in particular during glacial episodes.

5. Conclusions

We present the first Fe–Mn crust records of the radiogenic Nd, Hf and Pb isotope evolution of deep waters in the Canada Basin of the Arctic Ocean. The crusts were collected from the Northwind Ridge and provide a 7 Myr record of weathering inputs as a function of major climatic changes. Beryllium isotopes were successfully applied to establish age models for the Fe–Mn crusts. The $^{10}Be/^{9}Be$ ratios at the surfaces of all crusts are systematically lower than modern bottom water values because the low growth rates result in average ratios and integration over time periods between 120 and 450 kyr of crust growth corresponding to up to four glacial/interglacial cycles. The data show that glacial deep-water $^{10}Be/^{9}Be$ ratios of the Late Quaternary must have been substantially lower than at present, in particular during glacial periods, which is consistent with previous findings in marine sediments from the Canada Basin.

The surface Nd and Hf isotope compositions of the crusts are in good agreement with modern deep waters. At about 4.5 to 4 Ma, coinciding with the earliest stages of the intensification of Northern Hemisphere Glaciation, the deep waters in the Canada Basin started a continuous change towards the present day unradiogenic Nd and Hf, as well as radiogenic Pb isotope signatures, which further steepened at ~1 Ma. For the past 4 Myr, the radiogenic isotope evolution of ADW in the Canada Basin closely resembled that of NADW, which demonstrates that similar drivers, i.e. mainly the change to alternating glacial and interglacial weathering regimes in northern North America in the course of the intensification of NHG and the repeated waxing and waning of continental ice sheets were responsible for this major change.

The trend towards less radiogenic ε_{Hf} values over time was most likely caused by increased mechanical weathering of zircons from the old cratonic continental crust and the amplitude of change (5 to 8 ε_{Hf} units) was somewhat more pronounced in the Arctic than in the Atlantic Ocean, possibly caused by the proximity of the Arctic crusts to the weathering sources and the restricted deep water exchange of the Arctic basin. Relative changes of up to 3 ε_{Nd} units in both the deep North Atlantic and the Arctic Ocean were of similar amplitude, whereas the absolute values are different by about 2 ε_{Nd} units reflecting the overall less radiogenic Nd isotope composition of NADW.

This study demonstrates that the change from more chemical weathering conditions to a regime dominated by physical, glacial weathering on the adjacent North American continent controlled the isotopic evolution in the deep Canada Basin of the Arctic Ocean. This is in contrast to the isotopic evolution of shallower Arctic Intermediate Water obtained from sediments on the Lomonosov Ridge, which has mainly been controlled by changes in inputs of Atlantic waters, as well as weathering processes and contributions from Eurasia and Siberia. This suggests that, unlike today, pronounced isotopic differences between the bottom water masses from different depths and areas of the Arctic Ocean linked to the continental input sources and the proximity to glaciated areas prevailed for most of the past 7 Myr, in particular the last ca. 4 Myr.

Acknowledgements

We would like to thank Albert Galy and two anonymous reviewers for their constructive reviews and Jean Lynch-Stieglitz for editorial handling. We thank the U.S. Extended Continental Shelf program for providing the samples used in this study, especially the Department of State as lead agency (Brian van Pay), the U.S. Geological Survey (Deborah Hutchinson and Brian Buczhowski), and NOAA (Carla Moore). The IGSN numbers of the three samples analyzed and the dredge hauls from which they were collected are: DS1-001 (ECS008001; dredge ECS000008), DS2-006G (ECS00006N; dredge ECS000009), and DS4-006B (ECS009064; dredge ECS000011).

Appendix A. Supplementary material

Supplementary material related to this article can be found online at http://dx.doi.org/10.1016/j.epsl.2015.03.007.

References

Aagaard, K., Coachman, L.K., Carmack, E., 1981. On the halocline of the Arctic Ocean. Deep Sea Research Part A. Oceanographic Research Papers 28 (6), 529–545.
Aagaard, K., Swift, J., Carmack, E., 1985. Thermohaline circulation in the Arctic Mediterranean Seas. J. Geophys. Res., Oceans (1978–2012) 90, 4833–4846.
Abouchami, W., Galer, S., Koschinsky, A., 1999. Pb and Nd isotopes in NE Atlantic Fe–Mn crusts: proxies for trace metal paleosources and paleocean circulation. Geochim. Cosmochim. Acta 63, 1489–1505.
Albarède, F., Simonetti, A., Vervoort, J.D., Blichert-Toft, J., Abouchami, W., 1998. A Hf–Nd isotopic correlation in ferromanganese nodules. Geophys. Res. Lett. 25, 3895–3898.
Albarède, F., Telouk, P., Blichert-Toft, J., Boyet, M., Agranier, A., Nelson, B., 2004. Precise and accurate isotopic measurements using multiple-collector ICPMS. Geochim. Cosmochim. Acta 68, 2725–2744.
AMAP, 1998. AMAP Assessment Report: Arctic Pollution Issues. Arctic Monitoring and Assessment Programme (AMAP), Oslo, Norway. 859 pp.
Andersson, P.S., Porcelli, D., Frank, M., Björk, G., Dahlqvist, R., Gustafsson, Ö., 2008. Neodymium isotopes in seawater from the Barents Sea and Fram Strfait Arctic–Atlantic gateways. Geochim. Cosmochim. Acta 72, 2854–2867.

Arsouze, T., Dutay, J.C., Lacan, F., Jeandel, C., 2009. Reconstructing the Nd oceanic cycle using a coupled dynamical-biogeochemical model. Biogeosciences 6, 2829–2846.

Backman, J., Moran, K., McInroy, D.B., Mayer, L.A., the Expedition 302 Scientists, 2006. Arctic coring expedition (ACEX). In: Proc. Integr. Ocean Drill. Program, vol. 302.

Backman, J., Jakobsson, M., Frank, M., Sangiorgi, F., Brinkhuis, H., Stickley, C., O'Regan, M., Løvlie, R., Pälike, H., Spofforth, D., Gattacecca, J., Moran, K., King, J., Heil, C., 2008. Age model and core-seismic integration for the Cenozoic Arctic Coring Expedition sediments from the Lomonosov Ridge. Paleoceanography 23, PA1S03. http://dx.doi.org/10.1029/2007PA001476.

Backman, J., Fornaciari, E., Rio, D., 2009. Biochronology and paleoceanography of late Pleistocene and Holocene calcareous nannofossil abundances across the Arctic Basin. Mar. Micropaleontol. 72, 86–98.

Bayon, G., Burton, K., Soulet, G., Vigier, N., Dennielou, B., Etoubleau, J., Ponzevera, E., German, C., Nesbitt, R., 2009. Hf and nd isotopes in marine sediments: constraints on global silicate weathering. Earth Planet. Sci. Lett. 277, 318–326.

von Blanckenburg, F., O'Nions, R.K., Hein, J.R., 1996. Distribution and sources of pre-anthropogenic lead isotopes in deep ocean water from Fe–Mn crusts. Geochim. Cosmochim. Acta 60, 4957–4963.

von Blanckenburg, F., Nägler, T.F., 2001. Weathering versus circulation-controlled changes in radiogenic isotope tracer composition of the Labrador Sea and North Atlantic Deep Water. Paleoceanography 16, 424–434.

Blichert-Toft, J., 2008. The Hf isotopic composition of zircon reference material 91500. Chem. Geol. 253, 252–257.

Bönisch, G., Schlosser, P., 1995. Deep water formation and exchange rates in the Greenland/Norwegian Seas and the Eurasian Basin of the Arctic Ocean derived from tracer balances. Prog. Oceanogr. 35, 29–52.

Burton, K.W., Ling, H.F., O'Nions, R.K., 1997. Closure of the Central American Isthmus and its effect on deep-water formation in the North Atlantic. Nature 386, 382–385.

Burton, K.W., Lee, D.C., Christensen, J.N., Halliday, A.N., Hein, J.R., 1999. Actual timing of neodymium isotopic variations recorded by Fe–Mn crusts in the Western North Atlantic. Earth Planet. Sci. Lett. 171, 149–156.

Chen, T.Y., Ling, H.F., Frank, M., Zhao, K.D., Jiang, S.Y., 2011. Zircon effect alone insufficient to generate seawater Nd–Hf isotope relationships. Geochem. Geophys. Geosyst. 12, Q05003. http://dx.doi.org/10.1029/2010GC003363.

Chen, T.Y., Frank, M., Haley, B.A., Gutjahr, M., Spielhagen, R.F., 2012. Variations of North Atlantic inflow to the Central Arctic Ocean over the last 14 million years inferred from hafnium and neodymium isotopes. Earth Planet. Sci. Lett. 353, 82–92.

Chen, T.Y., Li, G., Frank, M., Ling, H.-F., 2013. Hafnium isotope fractionation during continental weathering: implications for the generation of the seawater Nd–Hf isotope relationships. Geophys. Res. Lett. 40, 916–920.

Chmeleff, J., von Blanckenburg, F., Kossert, K., Jakob, D., 2010. Determination of the ^{10}Be half-life by multicollector ICP-MS and liquid scintillation counting. Nucl. Instrum. Methods Phys. Res., Sect. B, Beam Interact. Mater. Atoms 268, 192–199.

Christl, M., Vockenhuber, C., Kubik, P.W., Wacker, L., Lachner, J., Alfimov, V., Synal, H.A., 2013. The ETH Zurich AMS facilities: performance parameters and reference materials. Nucl. Instrum. Methods Phys. Res., Sect. B, Beam Interact. Mater. Atoms 294, 29–38.

Cohen, A., O'Nions, R., Siegenthaler, R., Griffin, W., 1988. Chronology of the pressure-temperature history recorded by a granulite terrain. Contrib. Mineral. Petrol. 98, 303–311.

Crocket, K.C., Vance, D., Foster, G.L., Richards, D.A., Tranter, M., 2012. Continental weathering fluxes during the last glacial/interglacial cycle: insights from the marine sedimentary Pb isotope record at Orphan Knoll, NW Atlantic. Quat. Sci. Rev. 38, 89–99.

Darby, D.A., 2014. Ephemeral formation of perennial sea ice in the Arctic Ocean during the middle Eocene. Nat. Geosci. 7, 210–213.

David, K., Frank, M., O'Nions, R.K., Belshaw, N.S., Arden, J.W., 2001. The Hf isotope composition of global seawater and the evolution of Hf isotopes in the deep Pacific Ocean from Fe–Mn crusts. Chem. Geol. 178, 23–42.

Driscoll, N.W., Haug, G.H., 1998. A short circuit in thermohaline circulation: a cause for northern hemisphere glaciation? Science 282, 436–438.

Eisenhauer, A., Spielhagen, R., Frank, M., Hentzschel, G., Mangini, A., Kubik, P., Dittrich-Hannen, B., Billen, T., 1994. ^{10}Be records of sediment cores from high northern latitudes: implications for environmental and climatic changes. Earth Planet. Sci. Lett. 124, 171–184.

Erel, Y., Harlavan, Y., Blum, J.D., 1994. Lead isotope systematics of granitoid weathering. Geochim. Cosmochim. Acta 58, 5299–5306.

Flesche Kleiven, H., Jansen, E., Fronval, T., Smith, T.M., 2002. Intensification of Northern Hemisphere glaciations in the circum Atlantic region (3.5–2.4 Ma)-ice-rafted detritus evidence. Palaeogeogr. Palaeoclimatol. Palaeoecol. 184, 213–223.

van de Flierdt, T., Frank, M., Lee, D.C., Halliday, A.N., 2002. Glacial weathering and the hafnium isotope composition of seawater. Earth Planet. Sci. Lett. 201, 639–647.

van de Flierdt, T., Frank, M., Halliday, A.N., Hein, J.R., Hattendorf, B., Günther, D., Kubik, P.W., 2004. Tracing the history of submarine hydrothermal inputs and the significance of hydrothermal hafnium for the seawater budget—a combined Pb–Hf–Nd isotope approach. Earth Planet. Sci. Lett. 222, 259–273.

Foster, G.L., Vance, D., 2006. Negligible glacial–interglacial variation in continental chemical weathering rates. Nature 444, 918–921.

Frank, M., 2002. Radiogenic isotopes: tracers of past ocean circulation and erosional input. Rev. Geophys. 40, 1001. http://dx.doi.org/10.1029/2000RG000094.

Frank, M., Eckhardt, J.D., Eisenhauer, A., Kubik, P.W., Dittrich-Hannen, B., Segl, M., Mangini, A., 1994. Beryllium 10, thorium 230, and protactinium 231 in Galapagos microplate sediments: implications of hydrothermal activity and paleoproductivity changes during the last 100 000 years. Paleoceanography 9, 559–578.

Frank, M., Whiteley, N., Kasten, S., Hein, J.R., O'Nions, R.K., 2002. North Atlantic Deep Water export to the Southern Ocean over the past 14 Myr: evidence from Nd and Pb isotopes in ferromanganese crusts. Paleoceanography 17, 1022. http://dx.doi.org/10.1029/2000PA000606.

Frank, M., Backman, J., Jakobsson, M., Moran, K., O'Regan, M., King, J., Haley, B.A., Kubik, P.W., Garbe-Schönberg, D., 2008. Beryllium isotopes in central Arctic Ocean sediments over the past 12.3 million years: stratigraphic and paleoclimatic implications. Paleoceanography 23, PA1S02. http://dx.doi.org/10.1029/2007PA001478.

Frank, M., Porcelli, D., Andersson, P., Baskaran, M., Björk, G., Kubik, P., Hattendorf, B., Guenther, D., 2009. The dissolved beryllium isotope composition of the Arctic Ocean. Geochim. Cosmochim. Acta 73, 6114–6133.

Galer, S., Abouchami, W., 1998. Practical application of lead triple spiking for correction of instrumental mass discrimination. Mineral. Mag. 62, 491–492.

Galer, S., O'Nions, R., 1989. Chemical and isotopic studies of ultramafic inclusions from the San Carlos Volcanic Field, Arizona: a bearing on their petrogenesis. J. Petrol. 30, 1033–1064.

Garbe-Schönberg, C.D., 1993. Simultaneous determination of thirty-seven trace elements in twenty-eight international rock standards by ICP-MS. Geostand. Newsl. 17, 81–97.

Gutjahr, M., Frank, M., Halliday, A.N., Keigwin, L.D., 2009. Retreat of the Laurentide ice sheet tracked by the isotopic composition of Pb in western North Atlantic seawater during termination 1. Earth Planet. Sci. Lett. 286, 546–555.

Gutjahr, M., Frank, M., Lippold, J., Halliday, A.N., 2014. Peak Last Glacial weathering intensity on the North American continent recorded by the authigenic Hf isotope composition of North Atlantic deep-sea sediments. Quat. Sci. Rev. 99, 97–111.

Haley, B.A., Frank, M., Spielhagen, R.F., Eisenhauer, A., 2008a. Influence of brine formation on Arctic Ocean circulation over the past 15 million years. Nat. Geosci. 1, 68–72.

Haley, B., Frank, M., Spielhagen, R., Fietzke, J., 2008b. Radiogenic isotope record of Arctic Ocean circulation and weathering inputs of the past 15 million years. Paleoceanography 23, PA1S13. http://dx.doi.org/10.1029/2007PA001486.

Haley, B.A., Polyak, L., 2013. Pre-modern Arctic Ocean circulation from surface sediment neodymium isotopes. Geophys. Res. Lett. 40, 893–897.

Haug, G.H., Ganopolski, A., Sigman, D.M., Rosell-Mele, A., Swann, G.E., Tiedemann, R., Jaccard, S.L., Bollmann, J., Maslin, M.A., Leng, M.J., Eglinton, G., 2005. North Pacific seasonality and the glaciation of North America 2.7 million years ago. Nature 433, 821–825.

Henken-Mellies, W., Beer, J., Heller, F., Hsü, K., Shen, C., Bonani, G., Hofmann, H., Suter, M., Wölfli, W., 1990. ^{10}Be and ^{9}Be in South Atlantic DSDP Site 519: relation to geomagnetic reversals and to sediment composition. Earth Planet. Sci. Lett. 98, 267–276.

Jacobsen, S.B., Wasserburg, G.J., 1980. Sm–Nd isotopic evolution of chondrites. Earth Planet. Sci. Lett. 50 (1), 139–155.

Jakobsson, M., Løvlie, R., Al-Hanbali, H., Arnold, E., Backman, J., Mörth, M., 2000. Manganese and color cycles in Arctic Ocean sediments constrain Pleistocene chronology. Geology 28, 23–26.

Jeandel, C., 1993. Concentration and isotopic composition of Nd in the Southern Atlantic Ocean. Earth Planet. Sci. Lett. 117, 581–591.

Jeandel, C., Bishop, J.K., Zindler, A., 1995. Exchange of neodymium and its isotopes between seawater and small and large particles in the Sargasso Sea. Geochim. Cosmochim. Acta 59, 535–547.

Knies, J., Mattingsdal, R., Fabian, K., Grøsfjeld, K., Baranwal, S., Husum, K., De Schepper, S., Vogt, C., Andersen, N., Matthiessen, J., Andreassen, K., Jokat, W., Nam, S.-I., Gaina, C., 2014. Effect of early Pliocene uplift on late Pliocene cooling in the Arctic–Atlantic gateway. Earth Planet. Sci. Lett. 387, 132–144.

Korschinek, G., Bergmaier, A., Faestermann, T., Gerstmann, U., Knie, K., Rugel, G., Wallner, A., Dillmann, I., Dollinger, G., von Gostomski, C., et al., 2010. A new value for the half-life of ^{10}Be by heavy-ion elastic recoil detection and liquid scintillation counting. Nucl. Instrum. Methods Phys. Res., Sect. B, Beam Interact. Mater. Atoms 268, 187–191.

Kraft, S., Frank, M., Hathorne, E.C., Weldeab, S., 2013. Assessment of seawater Nd isotope signatures extracted from foraminiferal shells and authigenic phases of Gulf of Guinea sediments. Geochim. Cosmochim. Acta 121, 414–435.

Kurzweil, F., Gutjahr, M., Vance, D., Keigwin, L., 2010. Authigenic Pb isotopes from the Laurentian fan: changes in chemical weathering and patterns of North American freshwater runoff during the last deglaciation. Earth Planet. Sci. Lett. 299, 458–465.

Lacan, F., Jeandel, C., 2004. Neodymium isotopic composition and rare earth element concentrations in the deep and intermediate Nordic seas: constraints

on the Iceland Scotland Overflow Water signatured Scotland Overflow Water signature. Geochem. Geophys. Geosyst. 5, Q11006. http://dx.doi.org/10.1029/2004GC000742.

Lacan, F., Jeandel, C., 2005a. Acquisition of the neodymium isotopic composition of the North Atlantic Deep Water. Geochem. Geophys. Geosyst. 6, Q12008. http://dx.doi.org/10.1029/2005GC000956.

Lacan, F., Jeandel, C., 2005b. Neodymium isotopes as a new tool for quantifying exchange fluxes at the continent–ocean interface. Earth Planet. Sci. Lett. 232, 245–257.

Lee, D.C., Halliday, A.N., Hein, J.R., Burton, K.W., Christensen, J.N., Günther, D., 1999. Hafnium isotope stratigraphy of ferromanganese crusts. Science 285, 1052–1054.

Lemmen, D.S., Duk-Rodkin, A., Bednarski, J.M., 1994. Late glacial drainage systems along the northwestern margin of the Laurentide Ice Sheet. Quat. Sci. Rev. 13, 805–828.

Ling, H.F., Burton, K.W., O'Nions, R.K., Kamber, B.S., Von Blanckenburg, F., Gibb, A.J., Hein, J.R., 1997. Evolution of Nd and Pb isotopes in Central Pacific seawater from ferromanganese crusts. Earth Planet. Sci. Lett. 146, 1–12.

Martin, E.E., Haley, B.A., 2000. Fossil fish teeth as proxies for seawater Sr and Nd isotopes. Geochim. Cosmochim. Acta 64, 835–847.

März, C., Schnetger, B., Brumsack, H.J., 2010. Paleoenvironmental implications of Cenozoic sediments from the Central Arctic Ocean (IODP Expedition 302) using inorganic geochemistry. Paleoceanography 25, PA3206. http://dx.doi.org/10.1029/2009PA001860.

Matthiessen, J., Knies, J., Vogt, C., Stein, R., 2009. Pliocene palaeoceanography of the Arctic Ocean and subarctic seas. Philos. Trans. R. Soc., Math. Phys. Eng. Sci. 367, 21–48.

Moran, K., et al., 2006. The Cenozoic palaeoenvironment of the Arctic Ocean. Nature 441, 601–605.

Muiños, S.B., Frank, M., Maden, C., Hein, J.R., Van de Flierdt, T., Lebreiro, S.M., Gaspar, L., Monteiro, J.H., Halliday, A.N., 2008. New constraints on the Pb and Nd isotopic evolution of NE Atlantic water masses. Geochem. Geophys. Geosyst. 9, Q02007. http://dx.doi.org/10.1029/2007GC001766.

Münker, C., Weyer, S., Scherer, E., Mezger, K., 2001. Separation of high field strength elements (Nb, Ta, Zr, Hf) and Lu from rock samples for MC-ICPMS measurements. Geochem. Geophys. Geosyst. 2, 1064. http://dx.doi.org/10.1029/2001GC000183.

Nowell, G.M., Kempton, P.D., Noble, S.R., Fitton, J.G., Saunders, A.D., Mahoney, J.J., Taylor, R.N., 1998. High precision Hf isotope measurements of MORB and OIB by thermal ionisation mass spectrometry: insights into the depleted mantle. Chem. Geol. 149 (3), 211–233.

O'Nions, R., Frank, M., von Blanckenburg, F., Ling, H.F., 1998. Secular variation of Nd and Pb isotopes in ferromanganese crusts from the Atlantic, Indian and Pacific Oceans. Earth Planet. Sci. Lett. 155, 15–28.

Piepgras, D.J., Wasserburg, G.J., 1987. Rare Earth element transport in the western North Atlantic inferred from Nd isotopic observations. Geochim. Cosmochim. Acta 51, 1257–1271.

Piotrowski, A.M., Lee, D.C., Christensen, J.N., Burton, K.W., Halliday, A.N., Hein, J.R., Günther, D., 2000. Changes in erosion and ocean circulation recorded in the Hf isotopic compositions of North Atlantic and Indian Ocean ferromanganese crusts. Earth Planet. Sci. Lett. 181, 315–325.

Polyak, L., Edwards, M.H., Coakley, B.J., Jakobsson, M., 2001. Ice shelves in the Pleistocene Arctic Ocean inferred from glaciogenic deep-sea bedforms. Nature 410, 453–457.

Porcelli, D., Andersson, P.S., Baskaran, M., Frank, M., Björk, G., Semiletov, I., 2009. The distribution of neodymium isotopes in Arctic Ocean basins. Geochim. Cosmochim. Acta 73, 2645–2659.

Raymo, M.E., 1994. The initiation of Northern Hemisphere glaciation. Annu. Rev. Earth Planet. Sci. 22, 353–383.

Rempfer, J., Stocker, T.F., Joos, F., Dutay, J.C., 2012. Sensitivity of Nd isotopic composition in seawater to changes in Nd sources and paleoceanographic implications. J. Geophys. Res., Oceans 117, C12010. http://dx.doi.org/10.1029/2012JC008161.

Reynolds, B., Frank, M., O'Nions, R., 1999. Nd- and Pb-isotope time series from Atlantic ferromanganese crusts: implications for changes in provenance and paleocirculation over the last 8 Myr. Earth Planet. Sci. Lett. 173, 381–396.

Rickli, J., Frank, M., Halliday, A.N., 2009. The hafnium–neodymium isotopic composition of Atlantic seawater. Earth Planet. Sci. Lett. 280, 118–127.

Rickli, J., Frank, M., Stichel, T., Bastian Georg, R., Vance, D., Halliday, A.N., 2012. Controls on the incongruent release of hafnium during weathering of metamorphic and sedimentary catchments. Geochim. Cosmochim. Acta 101, 263–284.

Riebe, C.S., Kirchner, J.W., Finkel, R.C., 2004. Erosional and climatic effects on long-term chemical weathering rates in granitic landscapes spanning diverse climate regimes. Earth Planet. Sci. Lett. 224 (3), 547–562.

Roberts, N.L., Piotrowski, A.M., McManus, J.F., Keigwin, L.D., 2010. Synchronous deglacial overturning and water mass source changes. Science 327, 75–78.

Rutberg, R.L., Hemming, S.R., Goldstein, S.L., 2000. Reduced North Atlantic Deep Water flux to the glacial Southern Ocean inferred from neodymium isotope ratios. Nature 405, 935–938.

Sellén, E., Jakobsson, M., Frank, M., Kubik, P.W., 2009. Pleistocene variations of beryllium isotopes in Central Arctic Ocean sediment cores. Glob. Planet. Change 68, 38–47.

Shackleton, N.J., Backman, J., Zimmerman, H., Kent, D.V., Hall, M.A., Roberts, D.G., Schnitker, D., Baldauf, J.G., Desprairies, A., Homrighausen, R., Huddlestun, P., Keene, J.B., Kaltenback, A.J., Krumsiek, K.A.O., Morton, A.C., Murray, J.W., Westberg-Smith, J., 1984. Oxygen isotope calibration of the onset of ice-rafting and history of glaciation in the North Atlantic region. Nature 307, 620–623.

Silver, L.T., Williams, I.S., Woodhead, J.A., 1984. Uranium in granites from the southwestern United States: actinide parent–daughter systems, sites and mobilization. Report of the Department of Energy (GJBX-45-81), 379 pp.

Stein, R., 2000. Circum-Arctic river discharge and its geological record: an introduction. Int. J. Earth Sci. 89, 447–449.

Stordal, M.C., Wasserburg, G.J., 1986. Neodymium isotopic study of Baffin Bay water: sources of REE from very old terranes. Earth Planet. Sci. Lett. 77 (3), 259–272.

Tanaka, T., Togashi, S., Kamioka, H., Amakawa, H., Kagami, H., Hamamoto, T., Yuhara, M., Orihashi, Y., Yoneda, S., Shimizu, H., et al., 2000. JNdi-1: a neodymium isotopic reference in consistency with LaJolla neodymium. Chem. Geol. 168, 279–281.

Vance, D., Teagle, D.A., Foster, G.L., 2009. Variable quaternary chemical weathering fluxes and imbalances in marine geochemical budgets. Nature 458, 493–496.

Vervoort, J.D., Patchett, P.J., Blichert-Toft, J., Albarède, F., 1999. Relationships between Lu–Hf and Sm–Nd isotopic systems in the global sedimentary system. Earth Planet. Sci. Lett. 168, 79–99.

White, W.M., Patchett, J., Ben Othman, D., 1986. Hf isotope ratios of marine sediments and Mn nodules: evidence for a mantle source of Hf in seawater. Earth Planet. Sci. Lett. 79, 46–54.

Winter, B.L., Johnson, C.M., Clark, D.L., 1997. Strontium, neodymium, and lead isotope variations of authigenic and silicate sediment components from the Late Cenozoic Arctic Ocean: implications for sediment provenance and the source of trace metals in seawater. Geochim. Cosmochim. Acta 61, 4181–4200.

Zachos, J., Pagani, M., Sloan, L., Thomas, E., Billups, K., 2001. Trends, rhythms, and aberrations in global climate 65 Ma to present. Science 292, 686–693.

Zimmermann, B., Porcelli, D., Frank, M., Rickli, J., Lee, D.C., Halliday, A.N., 2009a. The hafnium isotope composition of Pacific Ocean water. Geochim. Cosmochim. Acta 73, 91–101.

Zimmermann, B., Porcelli, D., Frank, M., Andersson, P.S., Baskaran, M., Lee, D.C., Halliday, A.N., 2009b. Hafnium isotopes in Arctic Ocean water. Geochim. Cosmochim. Acta 73, 3218–3233.